A&A 657, A55 (2022)
https://doi.org/10.1051/0004-6361/202142434

Astronomy & Astrophysics

Deexcitation rate coefficients of C_3 by collision with H_2 at low temperatures*

Carlos Santander[1], Otoniel Denis-Alpizar[2], and Carlos Cárdenas[3,4]

[1] Departamento de Física, Facultad de Ciencias Físicas y Matemáticas, Universidad de Chile, Santiago 837.0415, Chile
[2] Instituto de Ciencias Químicas Aplicadas, Facultad de Ingeniería, Universidad Autónoma de Chile, Av. Pedro de Valdivia 425, 7500912 Providencia, Santiago, Chile
e-mail: otoniel.denis@uautonoma.cl
[3] Departamento de Física, Facultad de Ciencias, Universidad de Chile, Casilla 653, Santiago 7800024, Santiago, Chile
[4] Centro para el Desarrollo de la Nanociencia y la Nanotecnología (CEDENNA), Avda. Ecuador 3493, Santiago 9170124, Chile
e-mail: cardena@uchile.cl

Received 14 October 2021 / Accepted 10 November 2021

ABSTRACT

Context. An accurate analysis of the physical-chemical conditions in the regions of the interstellar medium in which C_3 is observed requires knowing the collisional rate coefficients of this molecule with He, H_2, electrons, and H.
Aims. The main goals of this study are to present the first potential energy surface for the C_3 +H_2 complex, to study the dynamics of the system, and to report a set of rate coefficients at low temperature for the lower rotational states of C_3 with para- and ortho-H_2.
Methods. A large grid of ab initio energies was computed at the explicitly correlated coupled-cluster with single-, double-, and perturbative triple-excitation level of theory, together with the augmented correlation-consistent quadruple zeta basis set (CCSD(T)-F12a/aug-cc-pVQZ). This grid of energies was fit to an analytical function. The potential energy surface was employed in close-coupling calculations at low collisional energies.
Results. We present a high-level four-dimensional potential energy surface (PES) for studying the collision of C_3 with H_2. The global minimum of the surface is found in the linear HH-CCC configuration. Rotational deexcitation state-to-state cross sections of C_3 by collision with para- and ortho-H_2 are computed. Furthermore, a reduced two-dimensional surface is developed by averaging the surface over the orientation of H_2. The cross sections for the collision with para-H_2 using this approximation and those from the four-dimensional PES agree excellently. Finally, a set of rotational rate coefficients for the collision of C_3 with para- and ortho-H_2 at low temperatures are reported.

Key words. astrochemistry – molecular data – molecular processes – scattering – ISM: molecules

1. Introduction

Small carbon chains, such as C_2, C_3, and C_5, have been observed in several regions of the interstellar medium (ISM) (Souza & Lutz 1977; Giesen et al. 2020; Maier et al. 2001; Hinkle et al. 1988; Bernath et al. 1989). They are expected to be the building blocks of more complex organic molecules that could explain the origin of life. Furthermore, these molecules could form larger chains, such as polycyclic aromatic hydrocarbon (PAH) and fullerene, which are candidates for explaining some of the diffuse interstellar bands (DIBs) (Omont et al. 2019).

In typical molecular clouds, the density and temperature are low (10^2–10^4 cm^{-3} and 10–15 K). Therefore, the rotational population of the molecules detected cannot be described by a Boltzmann distribution. In these cases, an accurate analysis of the physical-chemical conditions of these regions should be made using nonlocal thermal equilibrium (non-LTE) models. These models require knowing the Einstein coefficients and state-to-state rate coefficients of the observed molecules with the most common colliders in the ISM. However, the rate coefficients for the collision with H_2, He, H, and e are not always available.

The C_3 molecule has no dipole moment, but it can be detected through its rovibrational transitions. Even in cases like this, knowing the rotational state-to-state rate coefficients is valuable. For example, due to the absence of specific rotational rate coefficients for C_3, the molecular abundance and excitation temperatures of this species in Sgr B2 and IRC+10216 were estimated by Cernicharo et al. (2000) using the rotational rates for OCS with H_2 within a given vibrational level, while those between the ground and bending states were the same rotational rates divided by 10. Furthermore, due to the lack of data for C_3 at that moment, Roueff et al. (2002) assumed the collisional rates to be proportional to the radiative line strengths in the analysis of the observation of C_3 in the translucent molecular cloud toward HD 210121, and concluded that it will be essential to understand the inelastic collisions with C_3 better.

The interaction of C_3 with He has been widely studied. Abdallah et al. (2008) computed a PES at the coupled-cluster with single-, double-, and perturbative triple-excitation level of theory (CCSD(T)) and reported the rate coefficients at low temperature, below 15 K, considering C_3 as a rigid rotor. More recently, Smith et al. (2014) presented a new PES calculated with the CCSDT(Q) method, using the rigid-monomer approximation. They extended the set of rate coefficients up to 100 K. Two PESs at the CCSD(T) and CCSD(T)-F12 level considering the bending angle of C_3 in the C_3 + He complex were also developed

* Tables 5 and 6 are only available at the CDS via anonymous ftp to cdsarc.u-strasbg.fr (130.79.128.5) or via http://cdsarc.u-strasbg.fr/viz-bin/cat/J/A+A/657/A55

(Denis-Alpizar et al. 2014; Al Mogren et al. 2014). Furthermore, the inclusion of the bending of C_3 in the close coupling calculations was investigated by Stoecklin et al. (2015). In this work, the cross sections computed using the rigid-rotor approximation and including the bending motion showed differences only for collisions energies higher than the bending frequency of C_3.

After the first studies of the collision C_3 with He, Schmidt et al. (2014) reported the detection of this molecule toward HD 169454. In the analysis of the data, these author employed the same approximation as Roueff et al. (2002) and also included the rates for C_3 + He (Abdallah et al. 2008), scaled to represent the collision with H_2, and the deexcitations from higher levels were fixed at values from rotational state $j = 10$ in the RADEX code (Van der Tak et al. 2007). The model using the new rates showed that a higher destruction rate is required to fit the observed column densities well. These authors also proposed that detailed research of collisional rates is necessary before the physical conditions of the molecular gas can be deduced in detail from the C_3 column densities.

The collision of C_3 with atomic hydrogen was studied recently by Chhabra and Dhilip Kumar (Chhabra & Dhilip Kumar 2019). These authors build a two-dimensional PES for the ground states of C_3 + H at the MRCI level and reported the rate coefficients up to 100 K. Even if the collision of C_3 with H_2 is nonreactive at low temperature (Mebel et al. 1998; Costes et al. 2006), no collisional rate coefficients have been reported so far. The rates for C_3 + para-H_2($j = 0$) can be estimated from those with He (Schöier et al. 2005). However, it has been shown that this approximation is not valid in all cases, and in general, it is not valid for collisions with ortho-H_2 (Kłos & Lique 2008; Vera et al. 2014; Denis-Alpizar et al. 2018). Therefore, the collision of C_3 with H_2 deserves to be investigated.

The main goals of this study are to present the first potential energy surface for the C_3 + H_2 complex, to study the dynamics of the system, and to report a set of rate coefficients at low temperature for the lower rotational states of C_3 with para- and ortho-H_2. This paper is organized as follows. In the next section, we present the methods we employed, and the results are discussed in Sect. 3. Finally, the main conclusions are summarized in Sect. 3.2.

2. Calculations

2.1. Ab initio calculations

The coordinates we employed to study the C_3 + H_2 complex are shown in Fig. 1. R connects the centers of mass of the H_2 and C_3 molecules, and θ_1, θ_2, and φ describe the angular orientations of both systems. C_3 and H_2 are considered rigid rotors in this work. The bond length of H_2 was taken as the vibrationally averaged value in the rovibrational ground state $r_{\text{H-H}} = 0.76664$ Å (Jankowski & Szalewicz 1998), while the distances between C=C were set to the equilibrium value of the C_3 molecule, $r_{\text{C-C}} = 1.277$ Å (Van Orden & Saykally 1998).

Table 1 shows the interaction energies computed using different methods and basis sets. The energies at the completed-basis-set (CBS) limit were estimated with the two-point extrapolation formula (Halkier et al. 1999), $E_{\text{CBS}} = \frac{E_X X^3 - E_Y Y^3}{X^3 - Y^3}$, where $X = 5$ and $Y = 4$ are the cardinality of the aug-cc-pV5Z, and aug-cc-pVQZ basis sets from CCSD(T) calculations. The CCSD(T)-F12a/aug-cc-pVQZ method gives energies close to the CBS limit at a relatively low computational cost. Therefore, all ab initio calculations were performed with this method as implemented in

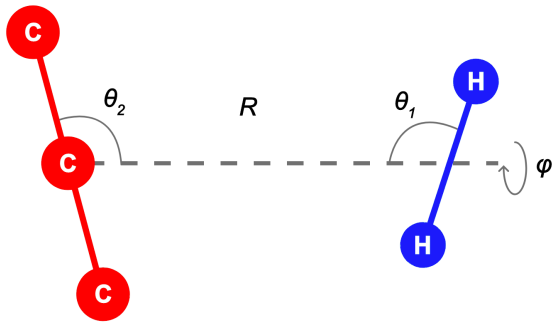

Fig. 1. Internal coordinates used to describe the C_3 + H_2 system. The azimuthal angle φ is undefined when either θ_1 or θ_2 is equal to 0° or 180°.

MOLPRO package (Werner et al. 2012). The size inconsistency of the CCSD(T)-F12a method was corrected by shifting up the ab initio interaction energies to make it vanish at $R = 200$ Å (Lique et al. 2010). The basis set superposition error was corrected using the counterpoise procedure of Boys and Bernardi (Boys & Bernardi 1970).

In total, 38 870 ab initio energies were computed. The radial coordinate R includes 23 values from 1.7 Å to 10.0 Å, while θ_1 and θ_2 vary from 0° to 180° in steps of 15°. The azimuthal angle φ varies in steps of 20° in the [0, 180]° interval.

2.2. Analytical four-dimensional surface

The grid of ab initio energies was fit following the same procedure as was recently used to study the HCO^+ + H_2 complex (Denis-Alpizar et al. 2020). The analytical function employed has the form

$$V(R,\theta_1,\theta_2,\varphi) = \sum_{l_1=0}^{12}\sum_{l_2=0}^{10}\sum_{m=0}^{\min(l_1,l_2,3)} f_m^{l_1,l_2}(R) \times \bar{P}_{l_1}^m(\cos\theta_1)\bar{P}_{l_2}^m(\cos\theta_2)\cos(m\varphi), \quad (1)$$

where the angular part is represented by a product of normalized associated Legendre polynomials and a cosine function. The molecules H_2 and C_3 have a center of symmetry; thus, l_1 and l_2 are restricted to even values (Nasri et al. 2015). For each value of R, the ab initio energies were fit using a least-squares method. Each coefficient $f_m^{l_1,l_2}(R)$ was then fit using the reproducing kernel Hilbert space (RKHS) procedure (Ho & Rabitz 1996),

$$f_m^{l_1,l_2}(R) = \sum_{k=1}^{N} \alpha_k^{l_1,l_2,m} q^{2,4}(R,R_k), \quad (2)$$

where N is the number of radial points of the grid (R_k). The $q^{2,4}(R,R_k)$ is the one-dimensional kernel, defined as

$$q^{2,4}(R_k,R) = \frac{2}{15R_>^5} - \frac{2R_<}{21R_>^6}, \quad (3)$$

$R_>$ and $R_<$ are the greater and lower value between the R_k and R. The $\alpha_k^{l_1,l_2,m}$ coefficients were found by solving the system of linear equations $\mathbf{q}(\mathbf{R}_i,\mathbf{R}_j)\alpha = \mathbf{f}_m^{l_1,l_2}(\mathbf{R}_i)$, where i and j label the different radial geometrical configurations of the grid.

Table 1. Interaction energy (in cm^{-1}) of H_2 with C_3 at the fixed angles ($\theta_1 = 0°$ and $\theta_2 = 90°$) for several values of R using different methods and basis sets (the aug-cc-pVXZ basis sets are represented as AVXZ).

Method/basis set	$R = 2.3$ Å	$R = 3.5$ Å	$R = 4.7$ Å	$R = 10$ Å	Time
CCSD(T)/AVTZ	3784.70	–23.55	–15.16	0.24	1
CCSD(T)/AVQZ	3703.23	–31.09	–15.60	0.23	4.13
CCSD(T)/AV5Z	3677.85	–33.14	–15.90	0.22	30.51
CCSD(T)/CBS limit	3651.22	–35.29	–16.21	0.22	35.64
CCSD(T)-F12a/AVTZ	3652.42	–34.42	–15.73	0.25	2.84
CCSD(T)-F12a/AVQZ	3651.49	–35.38	–15.97	0.23	7.66
CCSD(T)-F12b/AVTZ	3676.56	–31.46	–15.45	0.25	2.84
CCSD(T)-F12b/AVQZ	3664.02	–33.96	–15.84	0.23	6.75

Notes. The relative computational times are also shown.

2.3. Averaged surface

The use of a two-dimensional PES averaged over the orientation of H_2 to study the collision of a molecule with para-$H_2(j = 0)$ reduces computational cost in ab initio and dynamics calculations. This approximation has shown a reasonable agreement in the determination of the rate coefficients with those computed using the four-dimensional surface in several studies, for instance, SiS (Lique et al. 2008), HNC (Dumouchel et al. 2011), HCO^+ (Massó & Wiesenfeld 2014), and CF^+ (Desrousseaux et al. 2019). This is justified because in the dynamics of the collision with para-$H_2(j = 0)$, the coupling matrix elements are nonzero if $l_1 = 0$ (see Eq. (9) in Green 1975).

The four-dimensional PES can be averaged as

$$V_{\rm av}(R, \theta_2) = \langle Y^*_{j_1,k}(\theta_1, \varphi)|V(R, \theta_1, \theta_2, \varphi)|Y_{j_1,k}(\theta_1, \varphi)\rangle\,, \tag{4}$$

and if only the first rotational state of para-H_2 is considered, the rotational angular momentum of H_2, j_1, and its projection on the intermolecular axis, k, are equal to zero. This averaged PES can be obtained numerically by quadrature. However, this would require knowing the four-dimensional PES, and one of the goals of this approximation is to reduce the calculation times in the development of the PES. It has been shown that considering three orientations of H_2 is a good approximation to determine the averaged PES (Najar et al. 2014), and this is what we used here. The averaged energies were then computed as

$$E_{\rm av}(R, \theta_2) = \frac{1}{3}\{E(R, \theta_1 = 0°, \theta_2, \varphi = 0°) + E(R, \theta_1 = 90°, \theta_2, \varphi = 0°) + E(R, \theta_1 = 90°, \theta_2, \varphi = 90°)\}\,. \tag{5}$$

A grid of energies from Eq. (5), in the same intervals for R and θ_1 as were used for the four-dimensional PES, was then fit to the analytical expression

$$V_{\rm av}(R, \theta_2) = \sum_{l=1}^{12} f_l(R) P_k(\cos\theta_2). \tag{6}$$

For each value of R, the $f_l(R)$ coefficients were computed using a least-squares procedure. The $f_l(R)$ were then fit using the RKHS method, such as

$$f_l(R) = \sum_{k=1}^{N} \alpha^l_k q^{2,5}(R, R_k), \tag{7}$$

where $q^{2,5}(R, R_k)$ is the one-dimensional kernel (Ho & Rabitz 1996), defined as

$$q^{2,5}(R_k, R) = \frac{2}{21R^6_>} - \frac{1R_<}{14R^7_>}. \tag{8}$$

The subscript k corresponds to the k–ith radial point of the grid, and N is the number of R. $R_>$ and $R_<$ are the greater and lower value between the R_k and R. The α^l_k coefficients were obtained by solving the linear equations system $\mathbf{Q}(R_k, R_{k'})\alpha^l(R_{k'}) = \mathbf{f}(R_k)$, where $\mathbf{Q}(R_k, R_{k'}) = q^{2,5}(R_k, R_{k'})$, and k and k' label the geometrical configurations of the grid.

2.4. Scattering calculations

The four-dimensional PES was included in the Didimat code (Guillon et al. 2008) to study the collision of C_3 with para-H_2 and ortho-H_2. This code solves the close-coupling equations in the space-fixed frame. The log-derivative propagator (Manolopoulos 1988) was employed starting from $3\,a_0$. The minimum value of the maximum propagation distance was set to $60\,a_0$ and extended automatically. At each collision energy, the convergence of the quenching cross sections was checked as a function of the total angular momentum and maximum propagation distance. The rotational constants of H_2 and C_3 we used are $B_{H_2} = 60.853$ cm^{-1} (Huber & Herzberg 1979) and $B_{C_3} = 0.43057$ cm^{-1} (Van Orden & Saykally 1998). The inclusion of 18 rotational states of C_3 in the basis for the close-coupling calculation was enough to reach convergence. Table 2 shows the deexcitation cross sections for the collision with para-H_2 including one ($j_{H_2} = 0$) and two ($j_{H_2} = 0, 2$) rotational states in the basis at the collisional energies of 10 and 100 cm^{-1}. The cross sections with the two bases agree well at both energies. The average percent difference is lower than 4.2% at 10 cm^{-1} (this energy is in the region in which the resonances strongly affect the magnitude of the cross sections) and reduces to 2% at 100 cm^{-1}. Therefore, only one rotational state of H_2 was included in the basis to study the dynamics of the collision.

Furthermore, the averaged PES was employed to study the dynamics of the collision of C_3 with para-$H_2(j = 0)$. In this case, the code for investigating the atom-molecule collision, Newmat (Stoecklin et al. 2002), was used. The close-coupling equations were solved in the space-fixed frame, and the log-derivative propagator was also employed (Manolopoulos 1988). The minimum value of the largest propagation distance was 50 a_0 and was automatically extended. At each collisional energy, the convergence of the quenching cross section was checked as a function

Table 2. Rotational deexcitation cross sections (in a_0^2) of C_3 by collision with para-H_2 using one ($j_{H_2} = 0$) and two ($j_{H_2} = 0, 2$) states of H_2 in the dynamics calculations at collisional energies of 10 and 100 cm^{-1} for the lower transitions.

C_3 states		$E = 10\,cm^{-1}$		$E = 100\,cm^{-1}$	
$j_{initial}$	j_{final}	$j_{H_2} = 0$	$j_{H_2} = 0, 2$	$j_{H_2} = 0$	$j_{H_2} = 0, 2$
2	0	89.31	82.21	24.46	25.05
4	0	23.73	25.30	6.59	6.49
4	2	169.72	177.34	51.95	52.38
6	0	7.98	8.13	3.74	3.60
6	2	61.68	60.13	19.59	19.09
6	4	210.66	207.40	57.71	58.25

of the maximum intermolecular distance and the total angular momentum. In these calculations, 18 rotational states of C_3 were also considered.

Finally, the state-to-state deexcitation rate coefficients ($k_{j_i \to j_f}$) were computed by the average of the rotational cross sections ($\sigma_{j_i \to j_f}$) over a Maxwell-Boltzmann distribution at a given temperature T, as

$$k_{j_i \to j_f}(T) = \sqrt{\frac{8}{\pi \mu k_B^3 T^3}} \int_0^\infty \sigma_{j_i \to j_f}(E_c)\, E_c e^{-\frac{E_c}{k_B T}} dE_c, \quad (9)$$

where j_i and j_f are the initial and final rotational states of C_3, E_c is the collisional energy, and k_B is the Boltzmann constant.

3. Results and discussion

3.1. Potential energy surface

The quality of the fit of the four-dimensional PES was checked by evaluating the root-mean-square deviation (RMSD) of the ab initio energies of the grid and the fitted values. For $E \leq 0$ cm^{-1}, the RMSD was 6.19×10^{-2} cm^{-1}. In the intervals $0 \leq E \leq 1000$ cm^{-1}, $1000 \leq E \leq 5000$ cm^{-1}, and $5000 \leq E \leq 10\,000$ cm^{-1}, the RMSD were 0.155, 0.286, and 2.143 cm^{-1}, respectively.

Furthermore, a set of 987 ab initio energies (E_{ab}) not employed in the fitting procedure was computed. The averaged percentage difference between these energies and those (E_{ana}) computed with the analytical PES ($100 \times |(E_{ab} - E_{ana})/((E_{ab} + E_{ana})/2)$) for $E_{ab} < 5000$ cm^{-1} is lower than 2.6%, while in the $5000 \leq E_{ab} < 20\,000$ cm^{-1} interval, this values is 2.1%. Figure 2A shows the computed energies and the ab initio energies at geometrical configurations outside the grid that was used in the fit, which confirms that the agreement is very good. This figure also gives an indication of the anisotropy of the interaction.

The long range of the PES is also analysed from the multipolar expansion. The interaction energy can be written as the sum of the electrostatic (E_{elec}), induction (E_{ind}), and dispersion (E_{disp}) contributions, such as (Pullman 1978)

$$\begin{aligned} E_{elec} = {} & \frac{3\Theta^A_{zz}\Theta^B_{zz}}{4R^5}\Big(1 - 5\cos^2\theta_1 - 5\cos^2\theta_2 + 17\cos^2\theta_1\cos^2\theta_2 \\ & + 2\sin^2\theta_1\sin^2\theta_2\cos^2\varphi + 16\sin\theta_1\cos\theta_1\sin\theta_2\cos\theta_2\cos\varphi\Big) \\ & - 15\frac{\theta_1\Phi_2}{16R^7}\Big(1 - 7\cos^2\theta_1 - 14\cos^2\theta_2 + 21\cos^2\theta_2\cos^2\theta_2 \\ & + 74\cos^2\theta_1\cos^2\theta_2 - 91\cos^2\theta_1\cos^2\theta_2\cos^2\theta_2 \\ & + 4\sin^2\theta_1\sin^2\theta_2\cos^2\varphi(1 - 7\cos^2\theta_2) \\ & + 16\sin\theta_1\cos\theta_1\sin\theta_2\cos\theta_2\cos\phi(3 - 7\cos^2\theta_2)\Big) \\ & - 15\frac{\Phi_1\Phi_2}{16R^7}\Big(1 - 7\cos^2\theta_2 - 14\cos_2\theta_1 + 21\cos_2\theta_1\cos^2\theta_1 \\ & + 74\cos^2\theta_1\cos^2\theta_2 - 91\cos^2\theta_2\cos_2\theta_1\cos^2\theta_1 \\ & + 4\sin^2\theta_1\sin^2\theta_2\cos^2\phi(1 - 7\cos^2\theta_1) \\ & + 16\sin\theta_1\cos\theta_1\sin\cos\theta_2\cos\phi(3 - 7\cos^2\theta_2)\Big), \end{aligned} \quad (10)$$

$$E_{ind} = -\frac{9}{8R^8}(\Theta^A_{zz})^2\alpha^B(1 - 2\cos^2\theta_1 + 5\cos^4\theta_1), \quad (11)$$

and

$$\begin{aligned} E_{disp} = {} & \frac{3U_AU_B}{2(U_A + U_B)R^6}\left[\alpha^A\alpha^B + \frac{1}{3}\alpha^A(\alpha^B_{zz} - \alpha^B_{xx})\left(\frac{3}{2}\cos^2\theta_2 - \frac{1}{2}\right)\right. \\ & \left. + \frac{1}{3}\alpha^B(\alpha^A_{zz} - \alpha^A_{xx})\left(\frac{3}{2}\cos^2\theta_1 - \frac{1}{2}\right)\right], \end{aligned} \quad (12)$$

where $\alpha = (2\alpha_{xx} + \alpha_{zz})/3$ is a mean polarizability. Superscripts A and B denote the H_2 and C_3 molecules, respectively, and U is the ionization energy ($U_{H_2} = 15.426$ eV and $U_{C_3} = 13.0$ eV)

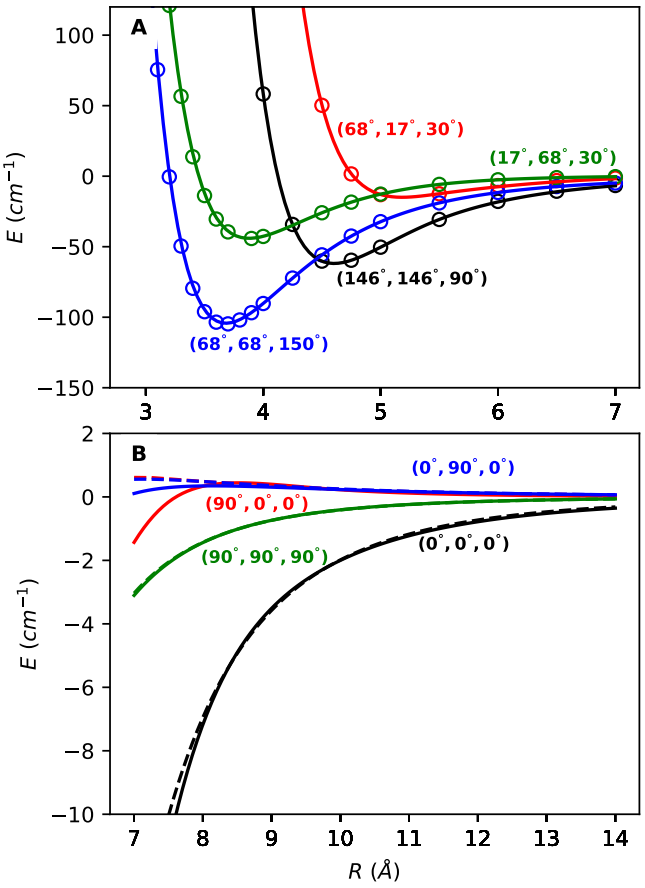

Fig. 2. Interaction energy along R of the C_3 + H_2 complex. *Panel A*: energies computed using the four-dimensional PES (solid lines) and from ab initio calculations (points) at several angular configuration (θ_1, θ_2, φ) of C_3 and H_2 that are not included in the grid used for the fit. *Panel B*: energies computed from the PES (solid lines) and analytical multipolar expansion (dashed line) at several angular configuration.

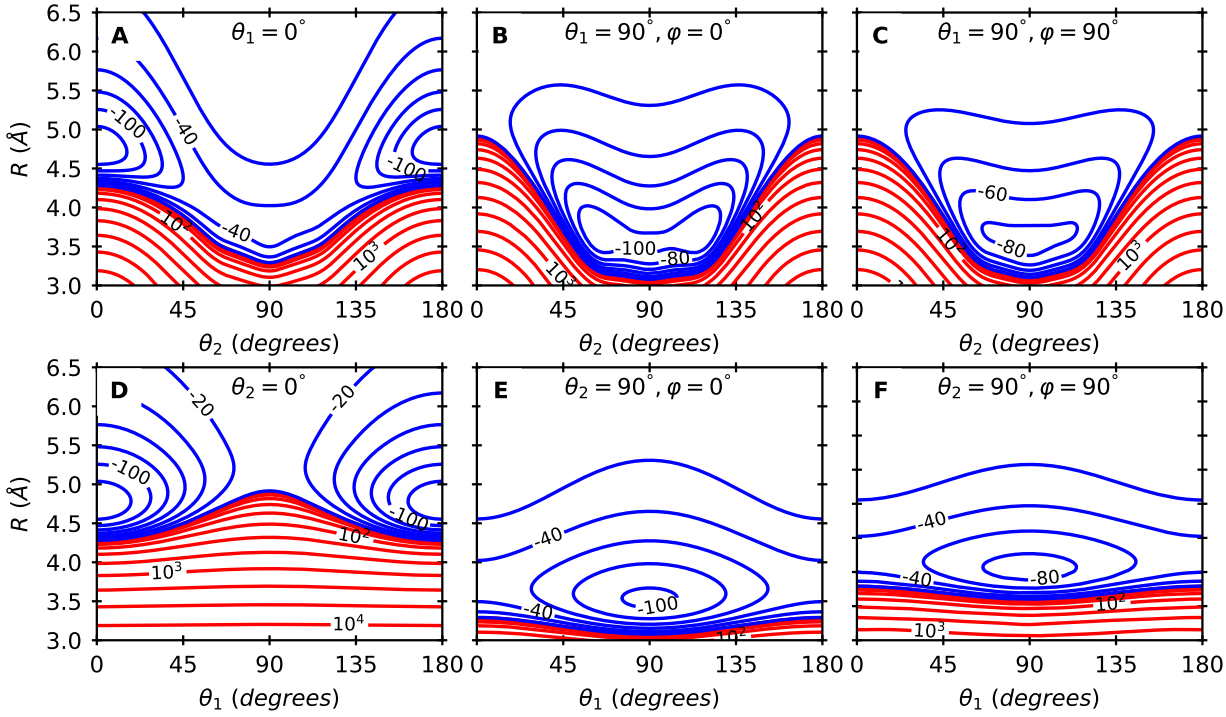

Fig. 3. Contour plot of the PES for the $C_3 + H_2$ complex at several geometrical configurations. Negative energies are represented as blue lines in steps 20 cm^{-1}. Positive energies (red lines) are logarithmically spaced between 1 cm^{-1} and 10^4 cm^{-1}.

Table 3. Molecular properties of C_3 and H_2 calculated at the CCSD(T)/aug-cc-pV5Z level using the finite-field method of Cohen and Roothaan[1].

Parameters	Definition	C_3	H_2
μ_z	Dipole moment	0	0
Θ_{zz}	Quadrupole moment	–4.22	0.45
Ω_{zzz}	Octupole moment	0	0
Φ_{zzzz}	Hexadecapole moment	–100.24	0.312
α_{xx}	Dipole polarizability	25.51	4.59
α_{zz}		51.11	6.44

Notes. All values are in a.u. [(1)](Cohen & Roothaan 1965).

(Johnson 2002). The computed molecular properties of C_3 and H_2 are listed in Table 3. Figure 2B shows the excellent agreement between the analytical multipolar energies and those from our PES. This makes this surface suitable for studying cold molecular collisions.

Figure 3 shows the contour plot of the analytical PES at several geometrical configurations. A strong dependence of the energies on the angular orientation is shown in this figure. The global minimum of the surface, named −135.64 cm^{-1}, was found at the $R = 4.76$ Å, in the linear configuration H–H–C–C–C, see panel A and D. This well is around 5 times deeper than the one found in C_3 + He (−25.87 cm^{-1} Abdallah et al. 2008, −25.54 cm^{-1} Zhang et al. 2009, −31.29 cm^{-1} Zhang et al. 2009, −26.73 cm^{-1} Denis-Alpizar et al. 2014 and −27.91 cm^{-1} Al Mogren et al. 2014).

Figure 3 also shows apparent local minima; see panels B, C, E, and F. However, Fig. 4 shows a contour plot in which R relaxes from 3.0 to 5.0 Å for $\varphi = 0^\circ$ and $\theta_1 = 90^\circ$. Only two secondary minima are observed in these figures: $E = -123.7$ cm^{-1} at $(\theta_1 = 69^\circ, \theta_2 = 122^\circ, \varphi = 0^\circ)$ and at symmetric configuration; and $E = -103.4$ cm^{-1} at $(\theta_1 = 90^\circ, \theta_2 = 90^\circ, \varphi = 0^\circ)$. A Fortran subroutine of this PES is available upon request to the authors or at the *github* link[1].

We also evaluated an averaged two-dimensional PES using the energies from Eq. (5). Figure 5 shows a contour plot of this surface. The minimum of this surface, −78.62 cm^{-1} was found at $\theta_2 = 90^\circ$, and $R = 3.6$ Å. This value is also higher than the value for the collision with He, but at the same T configuration. Additionally, an averaged PES was computed from Eq. (4) using a Gauss-Chebyshev quadrature of 20 points for the integration over φ and a Gauss–Legendre quadrature with 20 points over θ_1. This surface shows the same behavior as that of Fig. 5 (without visible differences). The minimum of this surface (−78.70 cm^{-1}) was found at the same geometrical configuration as the averaged PES shown in Fig. 5.

3.2. Dynamics

The four-dimensional PES presented in the previous section was employed in close-coupling calculations for collision energies from 10^{-2} up to 300 cm^{-1}. These calculations were performed for energies higher than the bending frequencies of C_3 ($\omega = 63$ cm^{-1}). In the study of the dynamics of C_3 in collision with He including the bending motion, the rotational deexcitation cross sections in the ground-vibrational state of the triatomic system agreed very well with those computed using the rigid-rotor approximation for energies lower than ω (Stoecklin et al. 2015). With increasing collisional energy, this good agreement between the two sets of cross sections decreases. For example, for the transition $4 \rightarrow 0$ at 200 cm^{-1}, the rigid-rotor approximation overestimated the cross section by 20% (Denis-Alpizar 2014). This difference is also observed in the rate coefficients.

[1] https://github.com/cjsantander/PES_H2-C3

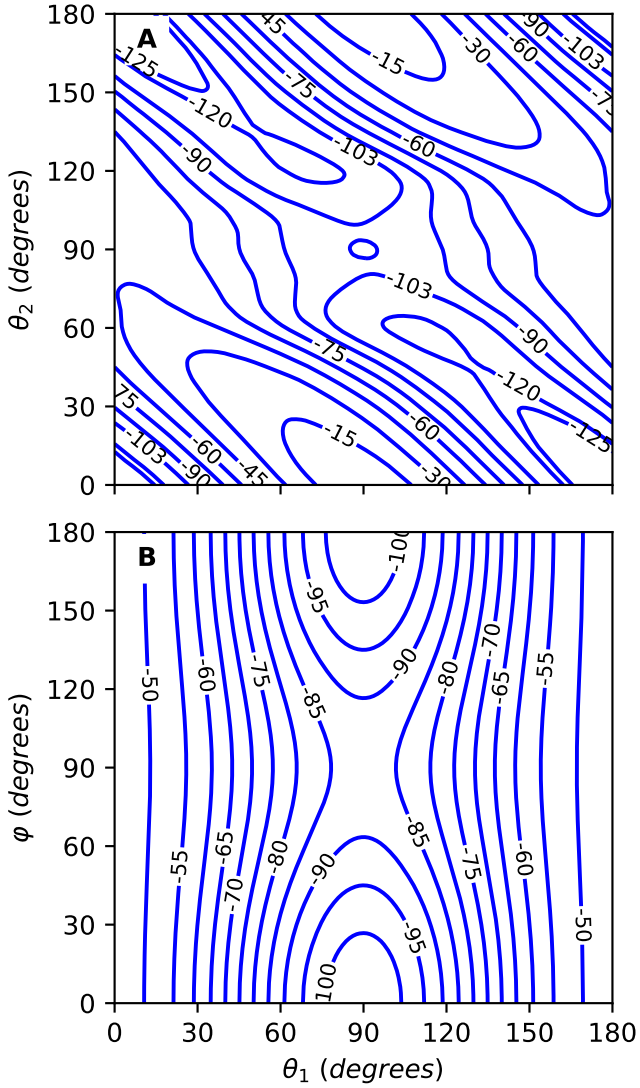

Fig. 4. Contour plot of the PES for the $C_3 + H_2$ complex. R is relaxed from 3.0 to 5.0 Å for $\varphi = 0°$ (*panel A*) and $\theta_2 = 90°$ (*panel B*). In the range $[-125, 0]$ cm^{-1}, the space between the lines is 15 cm^{-1} and 5 cm^{-1}.

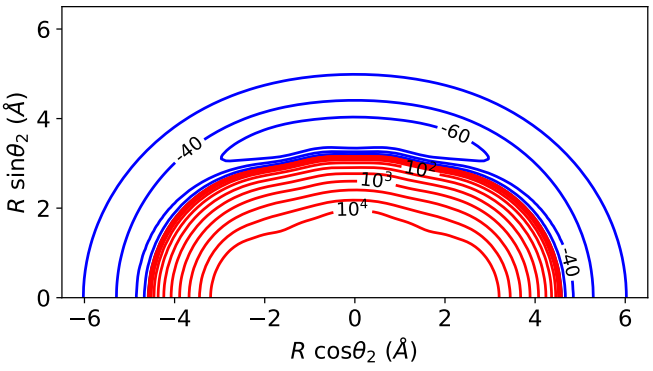

Fig. 5. Contour plot for the averaged PES of the $C_3 + H_2$ complex computed from Eq. (5). The space between blue lines is 20 cm^{-1} in the range $[-70, 0]$ cm^{-1}, and the red lines are logarithmically spaced between 1 cm^{-1} and 10^4 cm^{-1}.

At 50 K, the rates computed by Stoecklin et al. (2015) considering the molecule as a rigid rotor and including the bending motion of C_3 showed a percent difference of 21% (averaged over all deexcitation transitions for $j \leq 10$). This percent difference

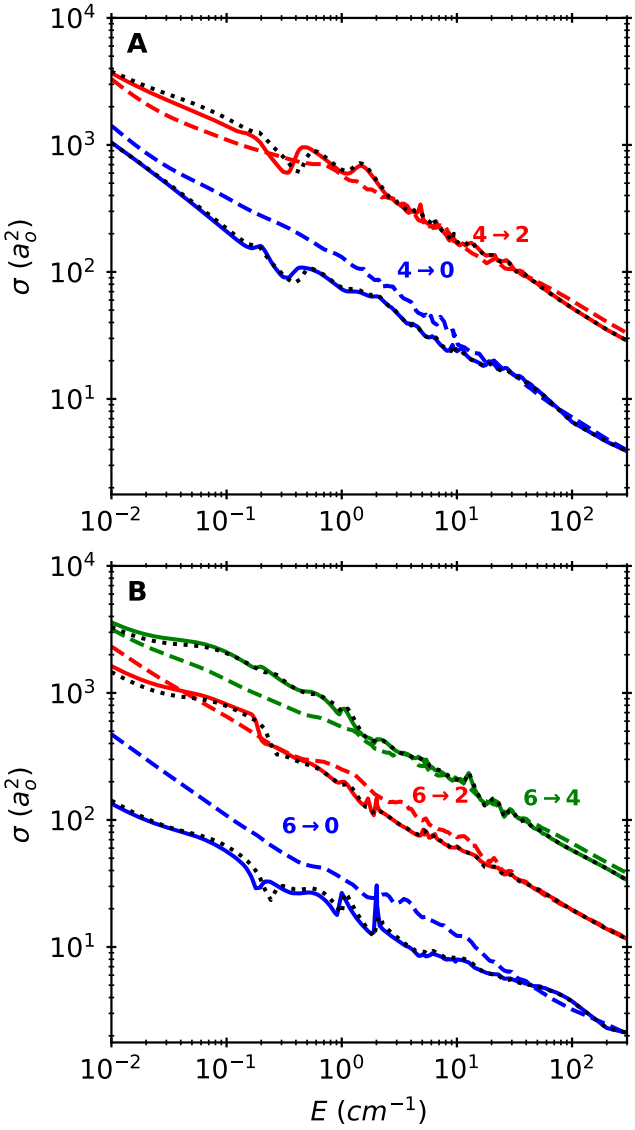

Fig. 6. Rotational deexcitations cross sections of C_3 from the initial rotational state $j = 4$ (*panel A*) and $j = 6$ (*panel B*), in collision with para-H_2 (solid lines), ortho-H_2 (dashed lines), and para-H_2 from averaged PES (dotted black lines). Rotational transitions of C_3 are labeled $j_i \rightarrow j_f$.

increases with increasing temperature. Therefore, we expect that considering the monomers as rigid rotors is a reasonably good approximation for collisional energies up to 300 cm^{-1}. In the case of $C_3 + H_2$, the PES is deeper than for C_3+He, and the bending-rotation coupling could be stronger. The cross sections at high collisional energies should be considered with caution.

Figure 6 shows the rotational cross sections for the collision of C_3 with para- and ortho-H_2. The cross sections decrease with increasing collision energy and $|\Delta j|$. The typical shape and Feshbach resonances, associated with the formation of quasi-bound states due to the PES centrifugal barrier and as a result of the coupling between open and closed channels (Yazidi et al. 2014), can also be observed in this figure.

The cross sections for the collision with para-H_2 from the averaged PES are also included in Fig. 6. These values agree very well with the cross sections computed using the four-dimensional PES. The use of a reduced PES has shown to be a reasonably good approximation for determining the

Table 4. Rotational deexcitation rate coefficients ($\times 10^{-11}$ cm^3 molecule^{-1} s^{-1}) of C_3 in collision with ortho-H_2, and para-H_2 at several temperatures.

j_i	j_f	oH$_2$	pH$_2$	He	oH$_2$	pH$_2$	He	H
$T = 5$ K					$T = 10$ K			
2	0	9.25	10.15	4.49	8.45	9.80	4.29	0.06
4	0	3.50	2.45	1.45	3.18	2.46	1.40	–
4	2	18.16	19.29	9.90	17.81	18.76	9.21	0.08
6	0	1.20	0.67	0.55	1.20	0.74	0.55	–
6	2	7.27	5.63	4.02	7.16	5.79	3.77	–
6	4	18.23	20.17	11.17	18.88	20.14	10.22	0.03
8	0	0.48	0.24	0.21	0.52	0.28	0.23	–
8	2	2.67	1.67	1.61	2.89	1.96	1.65	–
8	4	7.50	6.85	5.25	7.83	7.19	4.94	–
8	6	18.26	20.10	11.13	19.54	21.01	10.55	0.02
10	0	0.15	0.06	0.08	0.17	0.08	0.09	–
10	2	1.15	0.59	0.67	1.29	0.75	0.72	–
10	4	3.19	2.24	2.49	3.51	2.67	2.46	–
10	6	7.87	7.57	6.35	8.42	8.27	5.93	–
10	8	18.38	18.85	11.03	20.18	20.97	10.65	–
$T = 15$ K					$T = 20$ K			
2	0	8.24	9.81	4.01	8.24	9.78	–	0.05
4	0	3.02	2.50	1.37	2.91	2.53	–	–
4	2	17.71	18.64	8.71	17.73	18.55	–	0.11
6	0	1.17	0.80	0.57	1.15	0.84	–	–
6	2	7.00	5.90	3.65	6.88	5.98	–	–
6	4	19.09	19.96	9.58	19.23	19.77	–	0.08
8	0	0.54	0.32	0.25	0.55	0.35	–	–
8	2	2.97	2.14	1.69	3.00	2.28	–	–
8	4	7.86	7.32	4.69	7.81	7.35	–	–
8	6	20.01	21.17	9.92	20.22	21.04	–	0.05
10	0	0.19	0.10	0.11	0.21	0.11	–	–
10	2	1.38	0.86	0.78	1.43	0.94	–	–
10	4	3.66	2.92	2.43	3.72	3.08	–	–
10	6	8.61	8.54	5.55	8.62	8.58	–	–
10	8	20.93	21.71	10.11	21.25	21.89	–	–

Notes. (1) Available data for the collision with He (Abdallah et al. 2008) and H (Chhabra & Dhilip Kumar 2019) are also included. (2) Tables with the rate coefficients for the collision of C_3 with para- and ortho-H_2 at the rotational transitions up to $j = 20$ and $T = 50$ K are available at the CDS.

rate coefficients in the study of the collision of other systems (SiS Lique et al. 2008, HNC Dumouchel et al. 2011, C_2H Dagdigian 2018, CF^+ Desrousseaux et al. 2019, N_2H^+ Balança et al. 2020, and HCO^+ Denis-Alpizar et al. 2020). The C_3 molecule is another case that shows that this is an attractive approximation for estimating the rate coefficients with para-H_2 at reduced computational cost.

A set of rate coefficients for the lower rotational states of C_3 (up to $j = 20$) for the collision with para- and ortho-H_2 was determined from the computed cross sections at temperatures lower than 50 K. These rates are reported in Table 4 and in the supplementary material. The difference between the rates with para- and ortho-H_2 is small. This behavior has recently been observed in the study of the collisions with H_2 of several systems, for instance, C_4H^- (Balança et al. 2021), HCO^+ (Denis-Alpizar et al. 2020), DCO^+ (Denis-Alpizar et al. 2020), N_2H^+ (Balança et al. 2020), SH^+ (Dagdigian 2019), CF^+ (Desrousseaux et al. 2019), C_3N^- (Lara-Moreno et al. 2019), C_6H^- (Walker et al. 2017), HC_3N (Wernli et al. 2007), and CN^- (Kłos & Lique 2011). At low temperatures, this is associated with the effects of the long-range part of the interaction outweighing those of the short range (Balança et al. 2021).

Furthermore, the rates for the collision with He determined by Abdallah et al. (2008) that are available in the Basecol database (Dubernet et al. 2013) and the rates for the collision with H, computed from the excitation rates from Chaabra and Dhilip Kumar (Chhabra & Dhilip Kumar 2019) using the principle of detailed balance, are also included in Table 4. The rates for the collision with He are lower than those for the collision with para- and ortho-H_2. The mass-scaling approximation for determining the rates for the collision with para-H_2 from those with He was evaluated. The ratio of the rates with para-H_2 and He is 1.40 at 5 K, 1.54 at 10 K, and 1.64 at 15 K. These values are close to the 1.4 scaling factor that is commonly employed (Schöier et al. 2005), but this ratio varies from 0.8 up to 2.4, and this approximation should be considered with cation for C_3. In the case of the collision with H, our rates are also higher. Chhabra and Dhilip Kumar (Chhabra & Dhilip Kumar 2019) found that the rates for H were lower than those for He, and they associated this behavior with the different PES and colliders. Finally, we expect that the new rate coefficients reported here will be useful in determining the interstellar conditions in the regions in which this molecule has been detected.

4. Conclusions

We developed the first four-dimensional PES for the C_3-H_2 complex. This surface was fit from a large grid of ab initio energies computed at the CCSD(T)-F12a/aug-cc-pVQZ level of theory. The global minimum of the surface was found in the linear CCC-HH configuration. This surface was employed in close-coupling calculations. The cross sections for the lower rotational states of C_3 in collision with H_2 were computed. Furthermore, an averaged PES over the orientation of H_2 was used to study the relaxation of C_3 with para-$H_2(j=0)$. The cross sections using this surface and those computed with the four-dimensional PES were found to agree very well. Finally, we reported a set of rate coefficients for the lower rotational states of C_3 with para- and ortho-H_2 at low temperature.

Acknowledgements. Support from projects CONICYT/FONDECYT/REGULAR/ Nos. 1200732 and 1181121 is gratefully acknowledged. This research was partially supported by the supercomputing infrastructure of the NLHPC (ECM-02). C.C. acknowledges Center for the Development of Nanoscience and Nanotechnology CEDENNA AFB180001

References

Abdallah, D. B., Hammami, K., Najar, F., et al. 2008, ApJ, 686, 379
Al Mogren, M. M., Denis-Alpizar, O., Abdallah, D. B., et al. 2014, J. Chem. Phys., 141, 044308
Balança, C., Scribano, Y., Loreau, J., Lique, F., & Feautrier, N. 2020, MNRAS, 495, 2524
Balança, C., Quintas-Sánchez, E., Dawes, R., et al. 2021, MNRAS, 508, 1148
Bernath, P. F., Hinkle, K. H., & Keady, J. J. 1989, Science, 244, 562
Boys, S. F., & Bernardi, F. 1970, Mol. Phys., 19, 553
Cernicharo, J., Goicoechea, J. R., & Caux, E. 2000, ApJ, 534, L199
Chhabra, S., & Dhilip Kumar T. J. 2019, J. Phys. Chem. A, 123, 7296
Cohen, H. D., & Roothaan, C. C. J. 1965, J. Chem. Phys., 43, S34
Costes, M., Daugey, N., Naulin, C., et al. 2006, Faraday Discuss. Chem. Soc., 133, 157
Dagdigian, P. J. 2018, J. Chem. Phys., 148, 024304
Dagdigian, P. J. 2019, MNRAS, 487, 3427
Denis-Alpizar, O. 2014, PhD thesis, Université de Bordeaux
Denis-Alpizar, O., Stoecklin, T., & Halvick, P. 2014, J. Chem. Phys., 140, 084316
Denis-Alpizar, O., Stoecklin, T., Guilloteau, S., & Dutrey, A. 2018, MNRAS, 478, 1811
Denis-Alpizar, O., Stoecklin, T., Dutrey, A., & Guilloteau, S. 2020, MNRAS, 497, 4276
Desrousseaux, B., Quintas-Sánchez, E., Dawes, R., & Lique, F. 2019, J. Phys. Chem. A, 123, 9637
Dubernet, M.-L., Alexander, M. H., Ba, Y. A., et al. 2013, A&A, 553, A50
Dumouchel, F., Kłos, J., & Lique, F. 2011, Phys. Chem. Chem. Phys., 13, 8204
Giesen, T. F., Mookerjea, B., Fuchs, G. W., et al. 2020, A&A, 633, A120
Green, S. 1975, J. Chem. Phys., 62, 2271
Guillon, G., Stoecklin, T., Voronin, A., & Halvick, P. 2008, J. Chem. Phys., 129, 104308
Halkier, A., Klopper, W., Helgaker, T., Jorgensen, P., & Taylor, P. R. 1999, J. Chem. Phys., 111, 9157
Hinkle, K. W., Keady, J. J., & Bernath, P. F. 1988, Science, 241, 1319
Ho, T. S., & Rabitz, H. 1996, J. Phys. Chem., 104, 2584
Huber, K. P., & Herzberg, G. 1979, Molecular Spectra and Molecular Structure. IV. Constants of Diatomic Molecules (New York: Van Nostrand Reinhold)
Jankowski, P., & Szalewicz, K. 1998, J. Chem. Phys., 108, 3554
Johnson, R. 2002, Computational Chemistry Comparison and Benchmark Database, NIST Standard Reference Database 101
Kłos, J., & Lique, F. 2008, MNRAS, 390, 239
Kłos, J., & Lique, F. 2011, MNRAS, 418, 271
Lara-Moreno, M., Stoecklin, T., & Halvick, P. 2019, MNRAS, 486, 414
Lique, F., Toboła, R., Kłos, J., et al. 2008, A&A, 478, 567
Lique, F., Kłos, J., & Hochlaf, M. 2010, Phys. Chem. Chem. Phys., 12, 15672
Maier, J. P., Lakin, N. M., Walker, G. A. H., & Bohlender, D. A. 2001, ApJ, 553, 267
Manolopoulos, D. E. 1988, PhD thesis, University of Cambridge
Massó, H., & Wiesenfeld, L. 2014, J. Chem. Phys., 141, 184301
Mebel, A., Jackson, W., Chang, A., & Lin, S. 1998, J. Am. Chem. Soc., 120, 5751
Najar, F., Abdallah, D. B., Spielfiedel, A., et al. 2014, Chem. Phys. Lett., 614, 251
Nasri, S., Ajili, Y., Jaidane, N.-E., et al. 2015, J. Chem. Phys., 142, 174301
Omont, A., Bettinger, H. F., & Tönshoff, C. 2019, A&A, 625, A41
Pullman, B., ed. 1978, Intermolecular Interactions: From Diatomics to Biopolymers (New York: John Wiley & Sons)
Roueff, E., Felenbok, P., Black, J., & Gry, C. 2002, A&A, 384, 629
Schmidt, M., Krełowski, J., Galazutdinov, G., et al. 2014, MNRAS, 441, 1134
Schöier, F. L., van der Tak, F. F. S., van Dishoeck, E. F., & Black, J. H. 2005, A&A, 432, 369
Smith, D. G. A., Patkowski, K., Trinh, D., et al. 2014, J. Phys. Chem. A, 118, 6351
Souza, S. P., & Lutz, B. L. 1977, ApJ, 216, L49
Stoecklin, T., Voronin, A., & Rayez, J. C. 2002, Phys. Rev. A, 66, 042703
Stoecklin, T., Denis-Alpizar, O., & Halvick, P. 2015, MNRAS, 449, 3420
Van der Tak, F., Black, J. H., Schöier, F., Jansen, D., & van Dishoeck, E. F. 2007, A&A, 468, 627
Van Orden, A., & Saykally, R. J. 1998, Chem. Rev., 98, 2313
Vera, M. H., Kalugina, Y., Denis-Alpizar, O., Stoecklin, T., & Lique, F. 2014, J. Chem. Phys., 140, 224302
Walker, K. M., Lique, F., Dumouchel, F., & Dawes, R. 2017, MNRAS, 466, 831
Werner, H.-J., Knowles, P. J., Knizia, G., Manby, F. R., & Schütz, M. 2012, WIREs Comput. Mol. Sci., 2, 242
Wernli, M., Wiesenfeld, L., Faure, A., & Valiron, P. 2007, A&A, 464, 1147
Yazidi, O., Ben Abdallah, D., & Lique, F. 2014, MNRAS, 441, 664
Zhang, G., Zang, D., Sun, C., & Chen, D. 2009, Mol. Phys., 107, 1541